ACCOUNTS of chemical research

Article

pubs.acs.org/accounts

An Open Canvas—2D Materials with Defects, Disorder, and Functionality

Published as part of the Accounts of Chemical Research special issue "2D Nanomaterials beyond Graphene".

Xiaolong Zou and Boris I. Yakobson*

Department of Materials Science and NanoEngineering, Department of Chemistry, and Smalley Institute for Nanoscale Science and Technology, Rice University, Houston, Texas 77005, United States

CONSPECTUS: While some exceptional properties are unique to graphene only (its signature Dirac-cone gapless dispersion, carrier mobility, record strength), other features are common to other two-dimensional materials. The broader family "beyond graphene" offers greater choices to be explored and tailored for various applications. Transition metal dichalcogenides (TMDCs), hexagonal boron nitride (*h*-BN), and 2D layers of pure elements, like phosphorus or boron, can complement or even surpass graphene in many ways and uses, ranging from electronics and optoelectronics to catalysis and energy storage. Their availability greatly relies on chemical vapor deposition growth of large samples, which are highly polycrystalline and include interfaces such as edges, heterostructures, and grain boundaries, as well as dislocations and point defects. These imperfections do not always degrade the material properties, but they often bring new physics and even useful functionality. It turns particularly interesting in combination with the sheer openness of all 2D sheets, fully exposed to the environment, which, as we show herein, can change and tune the defect structures and consequently all their qualities, from electronic levels, conductivity, magnetism, and optics to structural mobility of dislocations and catalytic activities.

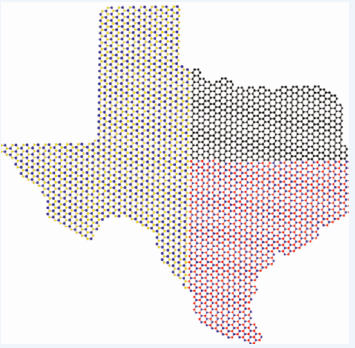

In this Account, we review our progress in understanding of various defects. We begin by expressing the energy of an arbitrary graphene edge analytically, so that the environment is regarded by "chemical phase shift". This has profound implications for graphene and carbon nanotube growth. Generalization of this equation to heteroelemental BN gives a method to determine the energy for arbitrary edges of BN, depending on the partial chemical potentials. This facilitates the tuning of the morphology and electronic and magnetic properties of pure BN or hybrid BN|C systems. Applying a similar method to three-atomic-layer TMDCs reveals more diverse edge structures for thermodynamically stable flakes. Moreover, CVD samples show new types of edge reconstruction, providing insight into the nonequilibrium growth process.

Combining dislocation theory with first-principles computations, we could predict the dislocation cores for BN and TMDC and reveal their variable chemical makeup. This lays the foundation for the unique sensitivity to ambient conditions. For example, partial occupation of the defect states for dislocations in TMDCs renders them intrinsically magnetic. The exchange coupling between electrons from neighboring dislocations in grain boundaries further makes them half-metallic, which may find its applications in spintronics.

Finally, brief discussion of monoelemental 2D-layer phosphorus and especially the structures and growth routes of 2D boron shows how theoretical assessment can help the quest for new synthetic routes.

■ INTRODUCTION

The exploration of graphene, and especially the snags in achieving the bandgap range coveted for electronics, has extended the attention to other two-dimensional (2D) materials. These include hexagonal boron nitride (*h*-BN), transition metal dichalcogenides (TMDCs) MX_2, and 2D atomic sheets of other elemental neighbors (P and, so far hypothetically, Si or B). They offer a broader palette of physical behaviors[1] for electronics and optoelectronics.[2] Moreover, their versatile chemistry and all-open double surface (area ∼1000−3000 m^2/g) invite new developments in catalysis, energy storage, and sensing.[3] For example, semiconducting MoS_2 in its 2H phase with sizable direct bandgap enables field effect transistors (FETs)[4] and phototransistors[5] with high performance; strained metallic WS_2 in 1T phase is catalytic for hydrogen evolution with very low overpotential;[6] insulating and chemically stable *h*-BN serves as high-temperature oxidation-resistant coating.[7]

One key to the exploitation of these diverse properties is in scalable methods to make the samples with rapid throughput. As developed for graphene growth,[8−11] chemical vapor deposition (CVD) has become the way to grow other large-scale 2D-crystal samples.[12−16] A direct consequence of nucleation, followed by growth and coalescence of multiple grains, is product polycrystallinity.[17,18] The CVD samples

Special Issue: 2D Nanomaterials beyond Graphene

Received: August 15, 2014
Published: December 16, 2014

DOI: 10.1021/ar500302q
Acc. Chem. Res. 2015, 48, 73−80

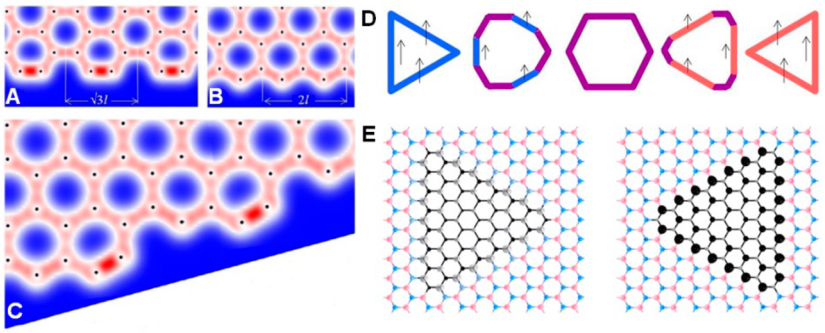

Figure 1. Electron density distribution is distinctly different for armchair (A) and zigzag (B) edges, with characteristic triple bonds forming along the armchair edge. The distinction remains in arbitrary slanted edge (C), illustrated by the computed electron density (from blue for zero to red for the highest value). Adapted from ref 21. Copyright 2010 The American Physical Society. (D) The equilibrium shapes of graphene inclusions, from triangle in N-rich conditions to nonagon and hexagon (nonmagnetic), and further to inverted nonagon and B-rich triangle again, computed for μ = −0.86, 0.42, 0.85, 1.55, and 2.69 eV. The colors mark the interface composition, red for ZB/C, purple for A/C, and blue for ZN/C; length of thin arrows is proportional to the magnetism. (E) Spin density for orientation-inverted graphene inclusions in BN matrix. Adapted from ref 26. Copyright 2011 American Chemical Society.

contain grains interfaced by 1D-formations: edges, heterostructures, and grain boundaries (GBs). They influence material properties;[13,14,19] their avoidance or purposeful engineering in controlled growth requires understanding of the origins, makeup, and functionalities of such "defects". Not only do they alter the properties of the sheet (lower strength, electronic mobility reduced by scattering), but they also can bring new functionalities, such as color centers (by permitting transitions distinctly different from "bulk"), imbedded electrical 1D-wires, magnetic centers, catalytic sites, etc. Further, according to Gibbs phase rule, the multielemental stoichiometry adds degrees of freedom and permits variation of the equilibrium composition (and properties) of defects, depending on ambient conditions. Combined with their sheer openness (essentially all-surface!), this brings about profoundly new behaviors of 2D-materials, an open canvas where different defect properties not only can be found but also can be reversibly altered, tuned by external factors (notably, chemical potential of constituent elements).

In this Account, we keep the above "open-canvas" perspective while describing mainly our laboratory's findings regarding the defects and properties. We begin with the edge of 2D islands, an ever-present "defect" akin to the surface of usual 3D-bulk. We introduce an energy decomposition *ansatz* allowing one to compute the energy of arbitrarily directed edges. We generalize this approach to binary *h*-BN, its edges, and BN−graphene interfaces, especially their dependence on chemical potentials, μ. Such dependence brought about by an added compositional degree of freedom (two elements in BN instead of just C alone) suggests an intriguing control of morphology and electronic and magnetic properties of BN or coplanar BN|C hybrids. Compared with BN, the MoS_2 flakes reveal more diverse edge structures, showing new edge reconstructions under S-poor conditions. Taking BN and MX_2 as examples, we combine the power of first-principles calculations with dislocation theory in predicting dislocation and GB precise structures and their variability and properties, not merely explaining experiments but rather guiding the search for unknown defects. Finally, we describe investigations on structures and possible growth methods of one hypothetical (not yet observed) material, pure-boron layer.

GRAPHENE, ISOMORPHIC *h*-BN, AND THEIR COPLANAR HETEROSTRUCTURES

A striking feature of most CVD samples is their rich morphology, delineated by the edges. In equilibrium, edge *energy* defines the shape (Wulff construction for crystals). In nonequilibrium growth, edge *kinetics* controls the shape. Edge energy is also important for coplanar interfaces, and for the brittle fracture.[20] Understanding of edges is the key to interpretation of observations and growth control.

Graphene serves as a monoelemental archetype to start with. An arbitrary edge is oriented at angle χ within $0° \le \chi \le 30°$, where 0° and 30° correspond to zigzag (Z) and armchair (A) edges. Although an arbitrary edge has rather random atom distribution, we could derive an analytic form for its energy $\gamma(\chi)$:[21]

$$\gamma(\chi) = 2\gamma_A \sin(\chi) + 2\gamma_Z \sin(30° - \chi) = |\gamma| \cos(\chi + C) \quad (1)$$

based on decomposition of the energy into contributions from A and Z segments. This is supported by the comparison of the charge density distribution for mixed chiral edge (Figure 1C) and those for pure A and Z edges (Figure 1A,B) and by matching to different levels of full computations.[21] It permits generalization to the dangling bonds of edges passivated by other elements, if adjusted by the cost μn of taking n terminating atoms from a reservoir of chemical potential μ:

$$\begin{aligned}\gamma(\chi) &= (\sqrt{3}\gamma_A - 2\gamma_Z) \sin(\chi - 30°) + (\gamma_A - 2\mu/\sqrt{3}) \\ &\quad \cos(\chi - 30°) \\ &= |\gamma'| \cos(\chi + C') \end{aligned} \quad (2)$$

The "chemical phase", $C'(\mu)$, captures the essential physics and accounts for different chemical environments of the edges. If the dangling bonds are terminated by catalytic metal, it resembles carbon nanotube (CNT)[21] or graphene growth.[8,10,22,23] The ability to change the chemical phase by tuning μ offers a way to control graphene shape or CNT chirality (complementing the structural CNT-catalyst matching[24]).

The expression 2 can be generalized to other 2D materials, such as BN or hybrid BN|C. There is an additional problem though. Unlike graphene, BN lacks the inversion symmetry,

DOI: 10.1021/ar500302q
Acc. Chem. Res. 2015, 48, 73−80

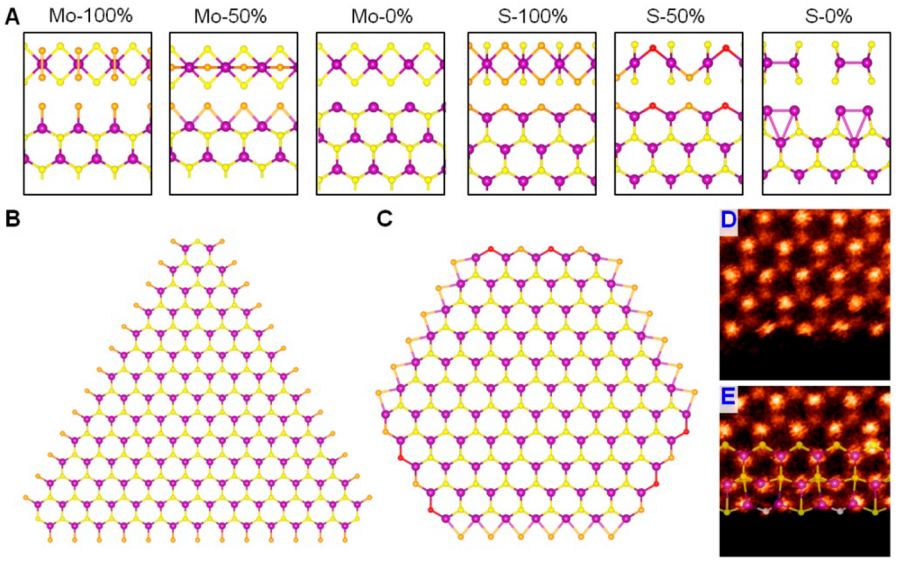

Figure 2. (A) Side view and top view of Mo and S edges with different S coverages. (B, C) Equilibrium shapes for MoS_2 islands under (B) synthesis or (C) HDS conditions. Purple and yellow represent Mo and S_2 atoms, respectively. Edge S atoms are highlighted in orange or red. Adapted from ref 28. Copyright 2002 Elsevier. (D, E) In CVD samples, Mo edge structures are observed with (D) 0% S coverage or (E) edge reconstruction due to S deficiency. In panel E, S atoms at the outmost row of the reconstructed edge are monosulfur rather than disulfur. Adapted from ref 35. Copyright 2013 American Chemical Society.

and the conventional way to define edge energy ceases to work: subtracting the energy of an equivalent amount of material in its 2D form from total energy of a Z ribbon (slab) yields only an inseparable sum of energies of the opposite B- and N-rich edges (ZB and ZN). A proposed alternative abandons the usual ribbon (slab) treatment but relies instead on intrinsic crystal symmetry (we used it earlier for 3D semiconductors[25]) and considers triangular BN flakes with all identical sides, either ZB or ZN. This allowed us to unambiguously calculate the μ-dependent γ_{ZB} and γ_{ZN}.[26] With γ_A (obtained by simple ribbon approach), γ_{ZB}, and γ_{ZN} all determined, the energy for an arbitrary edge under given conditions (given μ) is fully derived following the same logic as in obtaining eqs 1 and 2. This in turn permits prediction of the equilibrium shapes of BN flakes. Strikingly different from monoelemental graphene, the shapes now vary qualitatively with μ, as shown below for coplanar BN|C hybrids, rather interesting systems due to their tunable electronics and magnetism.

To obtain the interface energies, $\Gamma(\chi)$, in *hybrid* BN|C systems, the same scheme can be followed but at excessive cost of computing the series of large triangular inclusions. More efficiently, we utilize the energies already found for BN and C free edges, by properly subtracting the binding energy, E_{BN-C}, of joining into a heterostructure (binding energy being defined as the difference between the energies of separate islands with their edges and their joint system including the interface):[26]

$$\Gamma_{BN|C} = \gamma_{BN} + \gamma_C - E_{BN-C} \quad (3)$$

Since E_{BN-C} is independent of μ, $\Gamma(\chi)$ in the left-hand side varies with μ same way as γ_{BN} does. Direct use of Wulff construction reveals nontrivial morphology variation of graphene inclusions in a BN matrix (or BN in graphene) as μ changes. The shape varies from N-rich triangle to N-rich nonagon, to hexagon with A edges, then B-rich nonagon, and finally B-rich triangle (Figure 1D). Magnetic properties of these hybrids change accordingly. Since the magnetism is contributed by the π-electrons of carbon near the Z interfaces, the total magnetic moments equal the excess numbers of B or N atoms around the perimeter, following the Lieb's theorem.[27] Thin arrows in Figure 1D represent the cumulative spin around different inclusions; Figure 1E shows isodensity plots of spin for graphene inclusions of opposite orientations in BN. This demonstrates that interfacing graphene with BN opens rich possibilities for functional nanostructures with engineered electronic, magnetic, and optical properties.

EDGES OF THE TRIPLE-DECKER METAL DICHALCOGENIDE MONOLAYERS

Despite the similar binary composition to BN, transition metal dichalcogenides, MX_2, are three-atomic-layer sheets, consisting of a triangular M-layer in the middle, sandwiched between the two also triangularly packed X-layers. In 2H phase, the X atoms are arranged in trigonal prismatic geometry.[3] Chemically, the flexible coordination types of ligand X should bring in more variability of edges or other defects (such as dislocations discussed below), compared with sp^2-hybridized graphene or BN.

Previous work shows that TMDC edges can indeed vary,[28] displaying properties of interest, such as 1D metallicity,[29] ferromagnetism,[30] defect migration and rearrangement-slip deformation in WS_2 ribbons,[31] or enhanced photoluminescence along WS_2 edges.[19] They are catalytic for important reactions, including hydrogen evolution reaction[32,33] and hydrodesulfurization (HDS).[34] The triple-atomic-layer makeup allows the edges to have different chalcogenide coverage (abundance), as shown in Figure 2A for Mo- and S-directed edges of MoS_2 flakes. Adopting the method described above (for BN), the edge energies and Wulff construction can be calculated for MoS_2. Varying the sulfidation conditions brings interesting modification to the morphology of MoS_2 nanoparticles. At typical synthesis conditions (pure H_2S) or HDS working conditions, nanoparticles are triangular or truncated triangles (Figure 2B,C), respectively. The Mo edges for these thermodynamically stable islands have 100% or 50% S

DOI: 10.1021/ar500302q
Acc. Chem. Res. 2015, 48, 73−80

coverage. Differently, samples grown through a nonequilibrium CVD process often show a Mo edge with 0% S coverage (Figure 2D), despite its lower thermodynamic stability.[35] Additionally, a new type of S-poor Mo edge with reconstruction (Figure 2E) was observed, with single S vacancy at every S2 site along the regular Mo edge with 0% S coverage. Accordingly, the enhanced interaction between the two outmost rows of Mo induces strong reconstruction, with the outmost Mo atoms moved closer to the inner Mo row. This S-poor Mo edge represents perhaps an intermediate state during growth, and further supply of S would restore it back to a normal Mo edge with 0% S coverage. Better understanding the formation mechanisms is invaluable for the field, but the theory of TMDC (or BN) growth is still in its infancy. A nanoreactor diagram,[22] tracking the energy changes upon atom by atom accretion at the edge, is shown to be efficient in the case of carbon[24] and can be extended to other 2D materials, when more empirical reaction details become available.

BN GRAIN BOUNDARIES

Another class of interfaces ubiquitous in CVD samples are grain boundaries (GBs), naturally occurring as arrays of dislocations. Basic dislocations and GBs in graphene have been described earlier.[36−38] A pair of two basic disclinations, 5-pentagon and 7-heptagon, forms a dislocation in graphene (or nanotube[39]). The topological measure of a dislocation, Burgers vector **b**, depends on the spacing between 5 and 7. The smallest dislocation with **b** = (1, 0) consists of 5 and 7 sharing a C−C bond, a 5|7. Since the strain energy is typically proportional to $|\mathbf{b}|^2$, 5|7s are dominant in graphene. For BN, however, there is also "chemical" energy, originating from unfavorable homoelemental B−B or N−N bonds in any 5|7, while fully heteroelemental 4|8 (square−octagon pair) with **b** = (1, 1) carries greater strain energy. The delicate balance between the chemical and strain contributions defines which dislocations must be favored. By comparing dislocations with same |**b**| (a 4|8, split 5 and 7, and an adjacent pair of 5|7s), we find the 4|8 to be the most favorable structure.[40] This contrasts with graphene and 3D bulk materials where dislocations with larger **b** tend to split into weaker ones, with smaller **b**. The stabilization of 4|8 mainly arises from off-plane buckling.

The heteroelemental composition makes it necessary to classify bisector GBs into two groups by their mirror symmetry. These mirror-symmetric armchair A-GBs or asymmetric zigzag Z-GBs, can be generated through rotating two grains apart from either A or Z edge (see Figure 3). It has been found that low energy Z-GBs are composed of 4|8s, while favored A-GBs consist of 5|7s, and the latter have been observed indeed by ultrahigh-resolution transmission electron microscopy.[41] Of particular interest are the 60° and 180° Z-GBs, stitching together two fully inverted grains with a line of B−B or N−N bonds, respectively. Although morphologically identical with pristine lattice, the chemical polarity has important consequences, as previously shown in 2D cubic BN films.[42] Our results suggest that these polar GBs carry charge; moreover, their bandgap is significantly reduced with B−B and N−N bonds bringing unoccupied and occupied states into the bandgap near the conduction band minimum and the valence band maximum, respectively. Such GBs stand out as 1D nanowires imbedded in the insulating matrix.

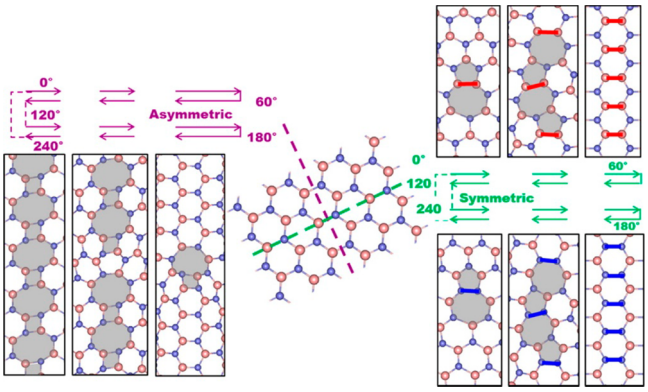

Figure 3. GB variability in 2D *h*-BN. The middle panel shows a perfect lattice, which can be thought of as two grains bonded seamlessly either along green or purple dashed lines. Rotation of two grains with respect to the green line leads to symmetric A-GBs (right panel), while rotation with respect to the purple line results in asymmetric Z-GBs (left panel). Reproduced from ref 40. Copyright 2012 American Chemical Society.

DISLOCATIONS AND GBS IN TRIPLE-DECKER METAL DICHALCOGENIDE MONOLAYERS

Compared with the monatomic BN case, the three-atomic-layer structure of TMDCs makes solving their dislocation structures more challenging. Combining the theory of dislocations and first-principles calculations, Zou et al. have predicted dislocation structures in TMDCs, revealing the diversity in chemical composition and its influences on electronics.[43] In MS_2 (M = Mo or W) as examples, deleting an armchair half-line of atoms in one of the opposite directions generates the smallest dislocations, either M-rich "⊥" or S-rich "⊤", shown leftmost in the top and bottom rows of Figure 4A. Although their planar view resembles 5|7 in BN, they extend in the third dimension across the complex TMDC layer, forming concave 3D polyhedra.

These dislocations interact effectively with point defects,[44] varying the internal makeup (and consequently all properties!). The top row of Figure 4A shows a series of reactions between ⊥ and one interstitial S, two interstitial S (equivalent to metal vacancy V_M), or four interstitial S (equivalent to substitution of one M with 2S), resulting in various derivative cores but unchanged **b**. Similarly, the bottom row in Figure 4A shows a series of reactions between ⊤ and one S vacancy V_S, two V_S (equivalent to interstitial M), or four V_S (equivalent to substitution of 2S with one M). The relative energies of these derivative cores with respect to basic ⊥ or ⊤ are calculated as functions of chemical potential of S (μ_S), Figure 4A. Surprisingly, almost all of these structures can be thermodynamically favored at certain μ_S. Two new cores turn up, composed of a hexagon−octagon pair (6|8) and a rhomb−hexagon pair (4|6). Most of these predicted structures have soon found confirmation in experiments by several groups.[13,14,35]

We now discuss the GBs built from dislocations. The bisector GBs can again be classified into A-GBs and Z-GBs, similar to those in BN. Figure 4B shows the GB energies, $G(\alpha)$, as functions of tilt angle α, for both A-GBs (bottom axis, red) and Z-GBs (top axis, blue). It should be emphasized that the tilt angle is set in the course of nonequilibrium growth processes, rather than determined by equilibrium energetics.[36] Therefore, the likelihood or the preference of specific GBs is determined

DOI: 10.1021/ar500302q
Acc. Chem. Res. 2015, 48, 73−80

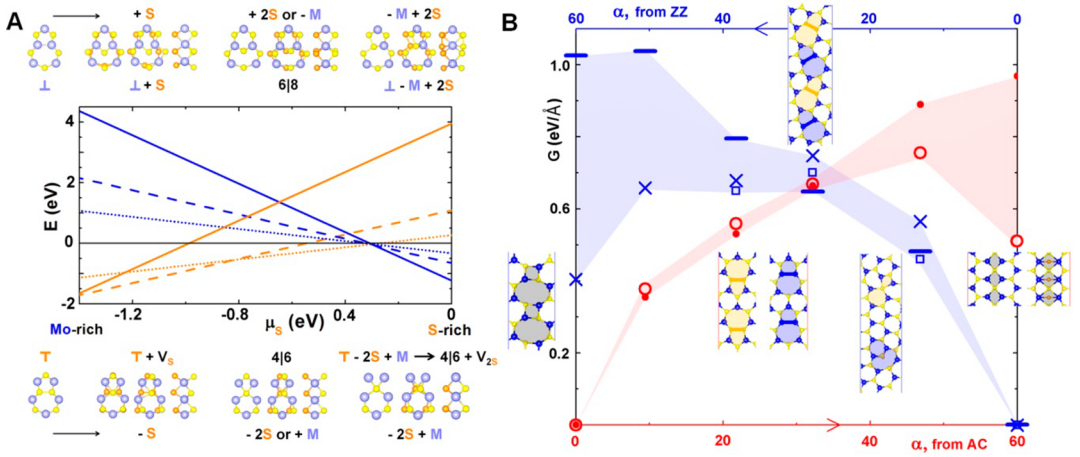

Figure 4. Dislocations and GBs in MoS_2. (A) (top and bottom) Dislocation cores derived from basic ones (⊥ or ⊤) through their reactions with point defects, as indicated by arrows. (middle) Energies of derivative cores with respect to ⊥ (blue lines) or ⊤ (orange lines) as functions of μ_S. The dotted, dashed, and solid lines with slopes 1, 2, and 4, correspond to structures in the top and bottom panels, from left to right. (B) GB energies as functions of tilt angle α, starting from either armchair (A-GBs, red) or zigzag (Z-GBs, blue), with their structures shown in the insets near the data points. Shaded areas represent the energy ranges due to reconstructions. Red solid circles are for A-GBs comprised of 5|7, and open circles are for A-GBs that consist of 4|6 and 6|8 gradually degenerating into all-rhombs GBs at 60°. Blue dashes, crosses, and open squares are for Z-GBs from 5|7, 4|8, and 4|6 + 6|8, respectively. Adapted from ref 43. Copyright 2012 American Chemical Society.

by the probability of local reconstructions or their interaction with point defects. Such probability is related to the difference in $G(\alpha)$ for different GBs at a preset α. The larger the difference, the higher the chance of "vertical" (at α = const) transitions down in energy. Figure 4B reveals distinct structural behaviors for GBs of different tilt. For low-angle GBs, the energy difference is so small that the probabilities of the formation of GBs composed of different cores make no big difference, while for high-angle (60°) GBs, the significant energy difference makes GBs composed of a line of rhombs (for A-GBs) or 4|8s (for Z-GBs) dominantly present in CVD samples.[13,35]

The variable dislocations/GBs can influence materials properties in many respects. Mechanically, their movements determine the deformation. Different dislocations follow distinct migration paths, with different barriers, and thus respond to stress differently. Figure 5 shows examples for 6|8 and 6|8 with one vacancy (6|8-V_S, V_S represents S vacancy) in WS_2. In both cases, the glide (A to C for 6|8-V_S, D to F for 6|8) involves the movement of W, indicated by blue circles. While no rearrangement of other atoms is needed for the glide of 6|8, the migration of additional S indicated by red circles is necessary to accommodate the glide of 6|8-V_S. Compared with the case of 6|8, the concerted migration of W and S atoms during the glide of 6|8-V_S results in greater distortion for the saddle-point structure and thus much larger migration barrier, Figure 5G. The migration of these dislocations has been observed.[45] Since the favorable dislocation structures are determined by chemical potential, notable difference in migration barriers suggests the possibility to tune mechanical properties of polycrystalline TMDC samples through environmental parameters. Electronically, two different behaviors emerge. Most GBs, including low-angle GBs and high-angle ones composed of 4|8s, introduce deep local states into the bandgap. These local states can deplete carriers, degrading the performance of FET devices made of CVD samples. In contrast, 60° A-GBs show dispersive bands around the Fermi level, thereby forming perfect metallic stripes in an otherwise semiconducting matrix. Careful engineering may bring about useful functionality adopting these uniquely imbedded metallic "wires".

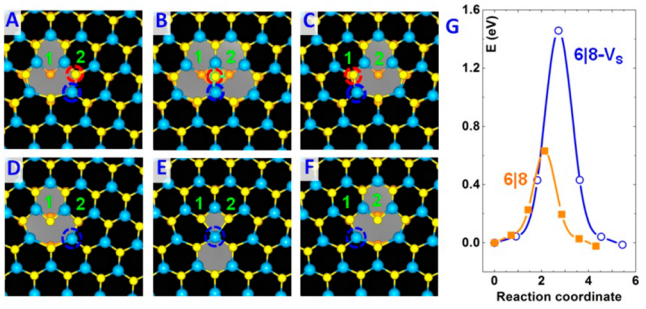

Figure 5. Dislocation migration in WS_2. Initial, saddle-point, and final structures for 6|8-V_S (A−C) and 6|8 (D−F). (G) Minimum energy paths for two migrating dislocations. Adapted from ref 45. Copyright 2014 Macmillan Publishers Limited.

Despite the usual detriment by GB localized states to device performance, they may also bring about exceptional properties. In particular, when these localized levels become partially occupied at some specific degree of doping, the system will undergo magnetic instability according to the Stoner model. Once the density of states (DOS) around the Fermi level is high enough, spin splitting occurs spontaneously, as demonstrated by Zhang et al.[46,47] Mo-rich ⊥ in a 9° GB introduces two localized levels, noted as δ and δ^* in Figure 6A. DOS analyses indicate that these states are mainly contributed by Mo $4d_{x^2-y^2,xy}$ and $4d_{z^2}$ with small mixing of S $3p_x$. The isodensity plots for these states further show that δ and δ^* have bonding and antibonding characteristics around the Mo−Mo bond, respectively. The nonmagnetic state with half-filled δ level is about 36 meV higher in energy than the spin-polarized state, causing the magnetism. Similar stabilization happens for ⊤, with δ^* half-filled in the nonmagnetic state. At a greater tilt angle, the increased overlap between electronic states from adjacent dislocations renders the localized levels more dispersive and the exchange splitting greater. This in turn leads to remarkable half

DOI: 10.1021/ar500302q
Acc. Chem. Res. 2015, 48, 73−80

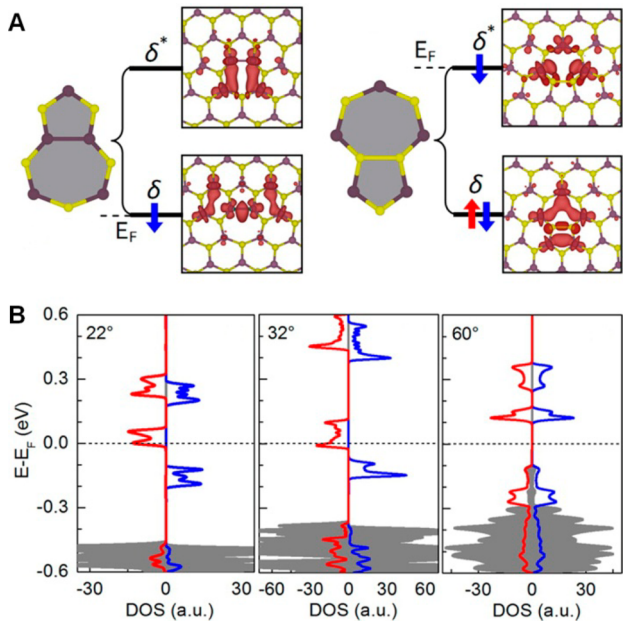

Figure 6. (A) Schematic energy levels of ⊥-induced (left) or ⊤-induced (right) spin-unpolarized localized states, δ and δ^*, and their corresponding isosurface (at 5×10^4 e/Å^3) of partial charge density distributions. Single arrow denotes a partially occupied energy level. (B) Spin-polarized density of states (DOS) for 22° and 32° GBs consisting of ⊥ as well as 60° GB comprised of 4|8s. Solid lines are the DOS projected onto atoms forming the GBs, while gray-shaded regions are the DOS projected onto atoms in bulk area. Adapted from ref 46. Copyright 2013 American Chemical Society.

metallicity in the range of $13° < \alpha \leq 32°$, as shown in the DOS plots in Figure 6B for two selected cases. Only above 47°, the favored GBs turn to composition of 4|8s and become antiferromagnetic. The revealed magnetism is significantly different from that in graphene, originating from imperfections that can be easily annealed or passivated, such as vacancies, adatoms, or edges. As topological defects, GBs cannot be annealed through local rearrangements. Their robust magnetism must be more beneficial for potential spintronics applications.

MONOELEMENTAL LAYERS OF P AND B

While above discussion was mostly concerned with mixed stoichiometries, the monoelemental noncarbon 2D materials also attract great attention. Among the properties of phosphorene (2D P), one important aspect that we have recently discovered[48] is its electrical robustness with respect to defects: edges, vacancies, dislocations, or GBs do not create midgap electronic states and thus are less detrimental for electronics. This advantage is important if tested in laboratories, since 2D P is practically available from naturally existing black phosphorus.

In contrast, monoelemental boron layers remain so far hypothetical. Close neighbor of C in the periodic table, with frustration due to electron deficiency, pure B solids show complex phase diagrams.[49] Our early prediction of the B_{80} fullerene[50] (with a B_{40} cage now found experimentally[51]) has motivated identification of the ground states of planar 2D B, mostly based on the triangular grid (Figure 7B, top panel, x = 0) with specific patterns of B vacancies, V_B (see ref 52). Rearranging V_B yields numerous configurations, impeding direct use of first-principles methods. Treating B layers as

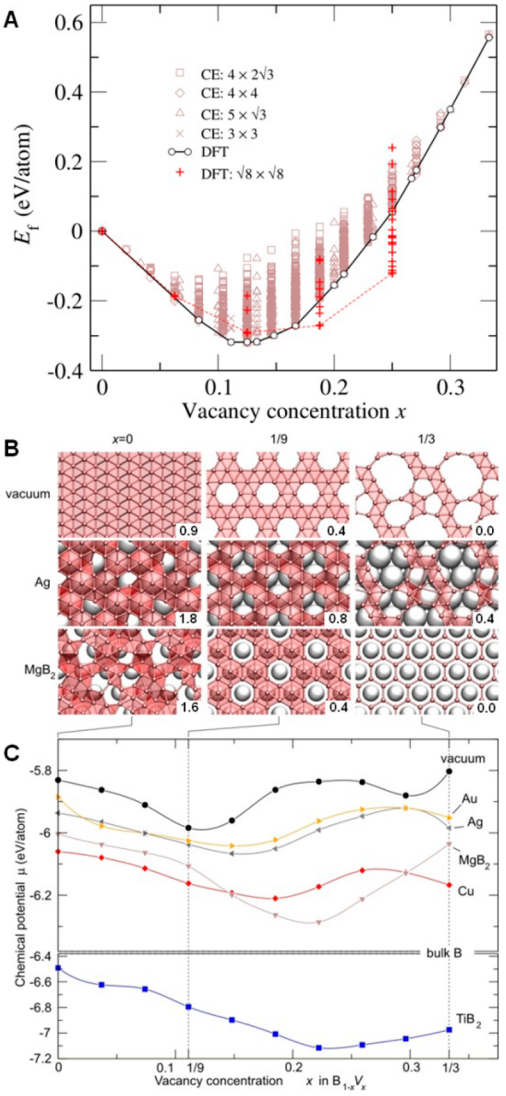

Figure 7. (A) Formation energies of 2D B with different vacancy fraction, x. Reproduced from ref 52. Copyright 2012 Wiley. (B) B sheets (x = 0, 1/9, and 1/3) in vacuum and on Ag(111) and Mg-terminated MgB_2(0001) surfaces. B is shown as a line network and the gray spheres are the metal topmost layer. (C) μ_{sheet} versus x, in vacuum and on surfaces. The vertical axis is broken at the μ of bulk α-boron. Panels B and C are adapted from ref 54. Copyright 2013 Wiley.

pseudoalloy $B_{1-x}V_{Bx}$, Penev et al. combined the cluster expansion and DFT methods to explore the configurational space.[52,53] Figure 7A summarizes the formation energies for about 2100 structures. Numerous B-layer phases could exist, including amorphous (top panel of Figure 7B, x = 1/3).

The polymorphism of B may complicate synthesis. Analyses of different growth methods (deposition, saturation, and evaporation) could suggest possible approaches. For the substrates, Liu et al. have studied Cu, Ag, and Au with low B solubility as well as MgB_2 and TiB_2, examples of non-transition-metal and transition-metal borides.[54] The $\mu_{adatoms} > \mu_{2D\text{-}cluster} > \mu_{sheet}$ provides the driving force for growth, and (except TiB_2) μ_{sheet} on all substrates exceeds μ of 3D bulk B, keeping 3D B thermodynamically favored; however, the high nucleation energy of 3D B could prevent its formation. The low B solubility and its fast diffusion on surfaces must facilitate the formation of 2D structures. The detailed calculations of

DOI: 10.1021/ar500302q
Acc. Chem. Res. 2015, 48, 73−80

adhesion energies suggest the deposition of B atoms on Au or Ag, or saturation of B-terminated MgB_2 surface as possible routes to grow 2D B.

CONCLUSIONS

While overviewing the progress in structures and physical properties of polycrystalline 2D materials, we focus on their imperfections: edges, dislocations, grain boundaries. One unifying theme in this Account was the variability of their properties, a distinct feature of all 2D materials due to their openness to the environment and therefore rapid adjustment to changes in thermodynamic conditions. We illustrate this behavior by the equilibrium morphology of the islands of BN or BN|C inclusions or MX_2 flakes and how it varies upon changes of chemical potentials of constituent elements. The correlation between morphology and chemical potential in hybrid BN|C systems or MX_2 offers a new way to control the electronic, magnetic, and catalytic properties. We further emphasize the same variability in the analysis of dislocations, while predicting their structures in BN and MX_2. Changes in chemical bonding result in significantly different properties of dislocations. Especially, the partial occupation of defect states in MX_2 renders the dislocations intrinsically magnetic. Our studies, along with findings in other laboratories, of monolayer phosphorus and of pure boron atomic layers illustrate new prospects in the monoelemental 2D family. Besides the pure 2D materials discussed above, the benefits from alloying or doping for engineering the diverse properties of MX_2[55] are further subjects of current development.

AUTHOR INFORMATION

Corresponding Author

*E-mail: biy@rice.edu.

Funding

This work was supported by the Department of Energy, BES Grant DE-SC0012547 (growth-edge analysis, boron, phosphorus), by the Army Research Office MURI Grant W911NF-11-1-0362 (metal chalcogenides), and in part by the Robert Welch Foundation (Grant C-1590).

Notes

The authors declare no competing financial interest.

Biographies

Xiaolong Zou received his Ph.D. (2011) in Physics from Tsinghua University, China. He is currently a Research Associate at Rice University, Houston, USA. Dr. Zou's current research focus is on 2D materials for new electronic and optical applications.

Boris I. Yakobson is the Hasselmann Chair in Engineering, Professor of Materials Science and Nano-Engineering, and Professor of Chemistry at Rice University. He received his Ph.D. in 1982 from the Russian Academy of Sciences, where he started his career. Prior to joining Rice in 1999, Yakobson was on the Physics faculty at North Carolina State University and a Visiting Scholar at the Department of Chemistry, Columbia University, New York, NY, in 1990.

REFERENCES

(1) Xu, X. D.; Yao, W.; Xiao, D.; Heinz, T. F. Spin and pseudospins in layered transition metal dichalcogenides. *Nat. Phys.* **2014**, *10*, 343−350.

(2) Wang, Q. H.; Kalantar-Zadeh, K.; Kis, A.; Coleman, J. N.; Strano, M. S. Electronics and optoelectronics of two-dimensional transition metal dichalcogenides. *Nat. Nanotechnol.* **2012**, *7*, 699−712.

(3) Chhowalla, M.; Shin, H. S.; Eda, G.; Li, L. J.; Loh, K. P.; Zhang, H. The chemistry of two-dimensional layered transition metal dichalcogenide nanosheets. *Nat. Chem.* **2013**, *5*, 263−275.

(4) Radisavljevic, B.; Radenovic, A.; Brivio, J.; Giacometti, V.; Kis, A. Single-layer MoS_2 transistors. *Nat. Nanotechnol.* **2011**, *6*, 147−150.

(5) Yin, Z. Y.; Li, H.; Li, H.; Jiang, L.; Shi, Y. M.; Sun, Y. H.; Lu, G.; Zhang, Q.; Chen, X. D.; Zhang, H. Single-layer MoS_2 phototransistors. *ACS Nano* **2012**, *6*, 74−80.

(6) Voiry, D.; Yamaguchi, H.; Li, J. W.; Silva, R.; Alves, D. C. B.; Fujita, T.; Chen, M. W.; Asefa, T.; Shenoy, V. B.; Eda, G.; Chhowalla, M. Enhanced catalytic activity in strained chemically exfoliated WS2 nanosheets for hydrogen evolution. *Nat. Mater.* **2013**, *12*, 850−855.

(7) Liu, Z.; Gong, Y. J.; Zhou, W.; Ma, L. L.; Yu, J. J.; Idrobo, J. C.; Jung, J.; MacDonald, A. H.; Vajtai, R.; Lou, J.; Ajayan, P. M. Ultrathin high-temperature oxidation-resistant coatings of hexagonal boron nitride. *Nat. Commun.* **2013**, *4*, No. 2541.

(8) Li, X. S.; Cai, W. W.; An, J. H.; Kim, S.; Nah, J.; Yang, D. X.; Piner, R.; Velamakanni, A.; Jung, I.; Tutuc, E.; Banerjee, S. K.; Colombo, L.; Ruoff, R. S. Large-area synthesis of high-quality and uniform graphene films on copper foils. *Science* **2009**, *324*, 1312−1314.

(9) Mattevi, C.; Kim, H.; Chhowalla, M. A review of chemical vapour deposition of graphene on copper. *J. Mater. Chem.* **2011**, *21*, 3324−3334.

(10) Kim, K. S.; Zhao, Y.; Jang, H.; Lee, S. Y.; Kim, J. M.; Kim, K. S.; Ahn, J. H.; Kim, P.; Choi, J. Y.; Hong, B. H. Large-scale pattern growth of graphene films for stretchable transparent electrodes. *Nature* **2009**, *457*, 706−710.

(11) Hao, Y.; Bharathi, M. S.; Wang, L.; Liu, Y.; Chen, H.; Nie, S.; Wang, X.; Chou, H.; Tan, C.; Fallahazad, B.; Ramanarayan, H.; Magnuson, C. W.; Tutuc, E.; Yakobson, B. I.; McCarty, K. F.; Zhang, Y.-W.; Kim, P.; Hone, J.; Colombo, L.; Ruoff, R. S. Large single crystal graphene growth on copper: The role of oxygen. *Science* **2013**, *342*, 720−723.

(12) Song, L.; Ci, L. J.; Lu, H.; Sorokin, P. B.; Jin, C. H.; Ni, J.; Kvashnin, A. G.; Kvashnin, D. G.; Lou, J.; Yakobson, B. I.; Ajayan, P. M. Large scale growth and characterization of atomic hexagonal boron nitride layers. *Nano Lett.* **2010**, *10*, 3209−3215.

(13) van der Zande, A. M.; Huang, P. Y.; Chenet, D. A.; Berkelbach, T. C.; You, Y. M.; Lee, G. H.; Heinz, T. F.; Reichman, D. R.; Muller, D. A.; Hone, J. C. Grains and grain boundaries in highly crystalline monolayer molybdenum disulphide. *Nat. Mater.* **2013**, *12*, 554−561.

(14) Najmaei, S.; Liu, Z.; Zhou, W.; Zou, X. L.; Shi, G.; Lei, S. D.; Yakobson, B. I.; Idrobo, J. C.; Ajayan, P. M.; Lou, J. Vapour phase growth and grain boundary structure of molybdenum disulphide atomic layers. *Nat. Mater.* **2013**, *12*, 754−759.

(15) Kim, K. K.; Hsu, A.; Jia, X. T.; Kim, S. M.; Shi, Y. S.; Hofmann, M.; Nezich, D.; Rodriguez-Nieva, J. F.; Dresselhaus, M.; Palacios, T.; Kong, J. Synthesis of monolayer hexagonal boron nitride on Cu foil using chemical vapor deposition. *Nano Lett.* **2012**, *12*, 161−166.

(16) Shi, Y. M.; Zhou, W.; Lu, A. Y.; Fang, W. J.; Lee, Y. H.; Hsu, A. L.; Kim, S. M.; Kim, K. K.; Yang, H. Y.; Li, L. J.; Idrobo, J. C.; Kong, J. van der Waals epitaxy of MoS_2 layers using graphene as growth templates. *Nano Lett.* **2012**, *12*, 2784−2791.

(17) Ajayan, P. M.; Yakobson, B. I. Graphene: Pushing the boundaries. *Nat. Mater.* **2011**, *10*, 415−417.

(18) Yazyev, O. V.; Chen, Y. P. Polycrystalline graphene and other two-dimensional materials. *Nat. Nanotechnol.* **2014**, *9*, 755−767.

(19) Gutierrez, H. R.; Perea-Lopez, N.; Elias, A. L.; Berkdemir, A.; Wang, B.; Lv, R.; Lopez-Urias, F.; Crespi, V. H.; Terrones, H.; Terrones, M. Extraordinary room-temperature photoluminescence in triangular WS_2 monolayers. *Nano Lett.* **2013**, *13*, 3447−3454.

(20) Kim, K.; Artyukhov, V. I.; Regan, W.; Liu, Y. Y.; Crommie, M. F.; Yakobson, B. I.; Zettl, A. Ripping graphene: Preferred directions. *Nano Lett.* **2012**, *12*, 293−297.

DOI: 10.1021/ar500302q
Acc. Chem. Res. 2015, 48, 73−80

(21) Liu, Y. Y.; Dobrinsky, A.; Yakobson, B. I. Graphene edge from armchair to zigzag: The origins of nanotube chirality? *Phys. Rev. Lett.* **2010**, *105*, No. 235502.
(22) Artyukhov, V. I.; Liu, Y. Y.; Yakobson, B. I. Equilibrium at the edge and atomistic mechanisms of graphene growth. *Proc. Natl. Acad. Sci. U.S.A.* **2012**, *109*, 15136−15140.
(23) Zhang, X. Y.; Li, H.; Ding, F. Self-assembly of carbon atoms on transition metal surfaces—Chemical vapor deposition growth mechanism of graphene. *Adv. Mater.* **2014**, *26*, 5488−5495.
(24) Artyukhov, V. I.; Penev, E. S.; Yakobson, B. I. Why do nanotubes grow chiral? *Nat. Commun.* **2014**, *5*, No. 4892.
(25) Rapcewicz, K.; Chen, B.; Yakobson, B.; Bernholc, J. Consistent methodology for calculating surface and interface energies. *Phys. Rev. B* **1998**, *57*, 7281−7291.
(26) Liu, Y. Y.; Bhowmick, S.; Yakobson, B. I. BN white graphene with "colorful" edges: The energies and morphology. *Nano Lett.* **2011**, *11*, 3113−3116.
(27) Wang, Z. J.; Qiu, X. M. Two theorems on the Hubbard-Hirsch model. *Commun. Theor. Phys.* **1997**, *28*, 51−56.
(28) Schweiger, H.; Raybaud, P.; Kresse, G.; Toulhoat, H. Shape and edge sites modifications of MoS_2 catalytic nanoparticles induced by working conditions: A theoretical Study. *J. Catal.* **2002**, *207*, 76−87.
(29) Bollinger, M. V.; Lauritsen, J. V.; Jacobsen, K. W.; Nørskov, J. K.; Helveg, S.; Besenbacher, F. One-dimensional metallic edge states in MoS2. *Phys. Rev. Lett.* **2001**, *87*, No. 196803.
(30) Li, Y.; Zhou, Z.; Zhang, S.; Chen, Z. MoS_2 nanoribbons: High stability and unusual electronic and magnetic properties. *J. Am. Chem. Soc.* **2008**, *130*, 16739−16744.
(31) Liu, Z.; Suenaga, K.; Wang, Z.; Shi, Z.; Okunishi, E.; Iijima, S. Identification of active atomic defects in a monolayered tungsten disulphide nanoribbon. *Nat. Commun.* **2011**, *2*, No. 213.
(32) Jaramillo, T. F.; Jørgensen, K. P.; Bonde, J.; Nielsen, J. H.; Horch, S.; Chorkendorff, I. Identification of active edge sites for electrochemical H_2 evolution from MoS_2 nanocatalysts. *Science* **2007**, *317*, 100−102.
(33) Hinnemann, B.; Moses, P. G.; Bonde, J.; Jørgensen, K. P.; Nielsen, J. H.; Horch, S.; Chorkendorff, I.; Nørskov, J. K. Biomimetic hydrogen evolution: MoS_2 nanoparticles as catalyst for hydrogen evolution. *J. Am. Chem. Soc.* **2005**, *127*, 5308−5309.
(34) Lauritsen, J. V.; Nyberg, M.; Nørskov, J. K.; Clausen, B. S.; Topsøe, H.; Laegsgaard, E.; Besenbacher, F. Hydrodesulfurization reaction pathways on MoS_2 nanoclusters revealed by scanning tunneling microscopy. *J. Catal.* **2004**, *224*, 94−106.
(35) Zhou, W.; Zou, X. L.; Najmaei, S.; Liu, Z.; Shi, Y. M.; Kong, J.; Lou, J.; Ajayan, P. M.; Yakobson, B. I.; Idrobo, J. C. Intrinsic structural defects in monolayer molybdenum disulfide. *Nano Lett.* **2013**, *13*, 2615−2622.
(36) Yakobson, B. I.; Ding, F. Observational geology of graphene, at the nanoscale. *ACS Nano* **2011**, *5*, 1569−1574.
(37) Liu, Y. Y.; Yakobson, B. I. Cones, pringles, and grain boundary landscapes in graphene topology. *Nano Lett.* **2010**, *10*, 2178−2183.
(38) Yazyev, O. V.; Louie, S. G. Topological defects in graphene: Dislocations and grain boundaries. *Phys. Rev. B* **2010**, *81*, No. 195420.
(39) Yakobson, B. I. Mechanical relaxation and "intramolecular plasticity" in carbon nanotubes. *Appl. Phys. Lett.* **1998**, *72*, 918−920.
(40) Liu, Y. Y.; Zou, X. L.; Yakobson, B. I. Dislocations and grain boundaries in two-dimensional boron nitride. *ACS Nano* **2012**, *6*, 7053−7058.
(41) Gibb, A. L.; Alem, N.; Chen, J. H.; Erickson, K. J.; Ciston, J.; Gautam, A.; Linck, M.; Zettl, A. Atomic resolution imaging of grain boundary defects in monolayer chemical vapor deposition-grown hexagonal boron nitride. *J. Am. Chem. Soc.* **2013**, *135*, 6758−6761.
(42) Zhang, Z. H.; Guo, W. L. Intrinsic metallic and semiconducting cubic boron nitride nanofilms. *Nano Lett.* **2012**, *12*, 3650−3655.
(43) Zou, X. L.; Liu, Y. Y.; Yakobson, B. I. Predicting dislocations and grain boundaries in two-dimensional metal-disulfides from the first principles. *Nano Lett.* **2013**, *13*, 253−258.
(44) Hirth, J. P.; Lothe, J. *Theory of Dislocations*, 2nd ed.; Wiley: New York, 1982.
(45) Azizi, A.; Zou, X. L.; Ercius, P.; H, Z. Z.; Elías, A. L.; Perea-López, N.; Stone, G.; Terrones, M.; Yakobson, B. I.; Alem, N. Dislocation motion and grain boundary migration in two-dimensional tungsten disulphide. *Nat. Commun.* **2014**, *5*, No. 4867.
(46) Zhang, Z. H.; Zou, X. L.; Crespi, V. H.; Yakobson, B. I. Intrinsic magnetism of grain boundaries in two-dimensional metal dichalcogenides. *ACS Nano* **2013**, *7*, 10475−10481.
(47) Joswig, J. O.; Lorenz, T.; Seifert, G. The virtues of magnetism. *ACS Nano* **2013**, *7*, 10449−10451.
(48) Liu, Y. Y.; Xu, F. B.; Zhang, Z. A.; Penev, E. S.; Yakobson, B. I. Two-dimensional mono-elemental semiconductor with electronically inactive defects: The case of phosphorus. *Nano Lett.* **2014**, *14*, 6782−6786 DOI: 10.1021/nl5021393.
(49) Oganov, A. R.; Chen, J. H.; Gatti, C.; Ma, Y. Z.; Ma, Y. M.; Glass, C. W.; Liu, Z. X.; Yu, T.; Kurakevych, O. O.; Solozhenko, V. L. Ionic high-pressure form of elemental boron. *Nature* **2009**, *457*, 863−867.
(50) Szwacki, N. G.; Sadrzadeh, A.; Yakobson, B. I. B-80 fullerene: An ab initio prediction of geometry, stability, and electronic structure. *Phys. Rev. Lett.* **2007**, *98*, No. 166804.
(51) Zhai, H. J.; Zhao, Y. F.; Li, W. L.; Chen, Q.; Bai, H.; Hu, H. S.; Piazza, Z. A.; Tian, W. J.; Lu, H. G.; Wu, Y. B.; Mu, Y. W.; Wei, G. F.; Liu, Z. P.; Li, J.; Li, S. D.; Wang, L. S. Observation of an all-boron fullerene. *Nat. Chem.* **2014**, *6*, 727−731.
(52) Penev, E. S.; Artyukhov, V. I.; Ding, F.; Yakobson, B. I. Unfolding the fullerene: Nanotubes, graphene and poly-elemental varieties by simulations. *Adv. Mater.* **2012**, *24*, 4956−4976.
(53) Penev, E. S.; Bhowmick, S.; Sadrzadeh, A.; Yakobson, B. I. Polymorphism of two-dimensional boron. *Nano Lett.* **2012**, *12*, 2441−2445.
(54) Liu, Y. Y.; Penev, E. S.; Yakobson, B. I. Probing the synthesis of two-dimensional boron by first-principles computations. *Angew. Chem., Int. Ed.* **2013**, *52*, 3156−3159.
(55) Kutana, A.; Penev, E. S.; Yakobson, B. I. Engineering electronic properties of layered transition-metal dichalcogenide compounds through alloying. *Nanoscale* **2014**, *6*, 5820−5825.

DOI: 10.1021/ar500302q
Acc. Chem. Res. 2015, 48, 73−80